

Dalton Transactions

Accepted Manuscript



This is an *Accepted Manuscript*, which has been through the Royal Society of Chemistry peer review process and has been accepted for publication.

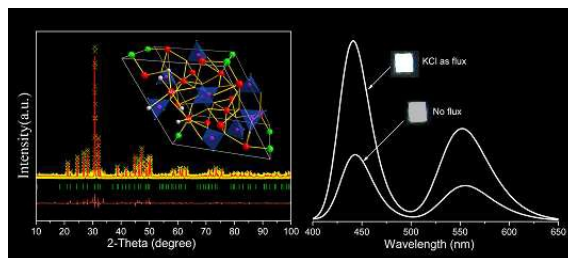
Accepted Manuscripts are published online shortly after acceptance, before technical editing, formatting and proof reading. Using this free service, authors can make their results available to the community, in citable form, before we publish the edited article. We will replace this *Accepted Manuscript* with the edited and formatted *Advance Article* as soon as it is available.

You can find more information about *Accepted Manuscripts* in the [Information for Authors](#).

Please note that technical editing may introduce minor changes to the text and/or graphics, which may alter content. The journal's standard [Terms & Conditions](#) and the [Ethical guidelines](#) still apply. In no event shall the Royal Society of Chemistry be held responsible for any errors or omissions in this *Accepted Manuscript* or any consequences arising from the use of any information it contains.

Graphic Abstract

A single-phased $\text{Sr}_5(\text{PO}_4)_3\text{F}:\text{Eu}^{2+}, \text{Mn}^{2+}$ phosphors are prepared. It exhibits broadband white-light emission under the near ultraviolet excitation. The emission color is modulated from blue to white. The photoluminescence intensity is enhanced by 85% using KCl as flux in the synthesis. The relation between photoluminescence with crystal and electronic structure are studied.



Enhancement of White-Light-Emission from Single-Phased $\text{Sr}_5(\text{PO}_4)_3\text{F}:\text{Eu}^{2+}$,
 Mn^{2+} Phosphor for Near-UV White LEDs

Yaomiao Feng, Jinping Huang*, Lili Liu, Jie Liu, Xibin Yu

*Shanghai Key Laboratory of Rare Earth Functional Materials, Department of
Chemistry, Shanghai Normal University, Shanghai 200234, China*

ABSTRACT A series of single-phased broadband white-light-emitting $\text{Sr}_5(\text{PO}_4)_3\text{F}:\text{Eu}^{2+}$, Mn^{2+} were prepared by solid state reaction. The luminescent property, crystal and electronic structure of the fluorophosphates were studied by photoluminescence, XRD Rietveld refinement and density functional theory calculation (DFT), respectively. Under the near ultraviolet excitation from 250 to 430 nm wavelength range, the phosphors exhibit two emission band centered at 440 and 556 nm contributed by Eu^{2+} and Mn^{2+} ions. By altering the relative ratio of Eu^{2+} to Mn^{2+} in the compound, the emission color could be modulated from blue to white. The efficient energy transfer from Eu^{2+} to Mn^{2+} ions could be ascribed to the well crystallized host lattice and the facile substitution of Eu^{2+} and Mn^{2+} for Sr^{2+} sites due to the similar ions radii. A series of fluxes were investigated to improve the photoluminescence intensity. When KCl was used as flux in the synthesis, the photoluminescence intensity of $\text{Sr}_5(\text{PO}_4)_3\text{F}:\text{Eu}^{2+}$, Mn^{2+} was enhanced by 85% compared with no fluxes added. These results demonstrate that the single-phased $\text{Sr}_5(\text{PO}_4)_3\text{F}:\text{Eu}^{2+}$, Mn^{2+} with the enhanced luminescent efficiency could be promising as near UV-convertible direct white-light-emitting phosphor for WLEDs application.

KEYWORDS White-light-emission; Single-phased phosphor; $\text{Sr}_5(\text{PO}_4)_3\text{F}:\text{Eu}^{2+}$, Mn^{2+} ; Flux; Luminescence enhancement.

* Corresponding author. E-mail address: hjinpj@shnu.edu.cn

1 Introduction

White-light-emitting diodes (WLEDs) are considered to be the 21st century green lighting source for solid state lighting due to the high energy efficiency, long operational lifetime, light stability and environmentally friendly characteristics.^{1,2} In the last two decades, much efforts have been devoted to application of WLEDs in display lighting sources and illuminating systems,^{3,4} in which search for novel phosphors with high efficiency, excellent chemical stability to improve the luminous efficiency of WLEDs devices is an imperative task, because the eventual performance of WLEDs devices mainly depends on the phosphors.⁵ The main approach to fabricate WLEDs devices is to combine a blue LEDs chip with a yellow-emitting phosphor $\text{Y}_3\text{Al}_5\text{O}_{12}:\text{Ce}^{3+}$ that has already been commercialized.⁶ However, white light generated by this kind of LEDs devices generally shows a poor color rendering index (CRI) and a high correlated color temperature (CCT) due to the deficiency of red component in the spectral region. An alternative method to combine near-ultraviolet (NUV) LEDs chips with trichromatic red, green and blue light-emitting phosphors has been proposed. Unfortunately, the phosphor mixture produces an inevitable problem of fluorescence re-absorption between different components and non-uniformity of luminescent properties, resulting in a loss of luminous efficiency and time-dependent shift of the color point. Consequently, exploration of single-phased white-light-emitting phosphors excited by near ultraviolet (NUV) light to improve the luminous efficiency and the color rendering index have gathered plenty of interests.⁷ By co-doping a sensitizer and an activator into the same crystalline matrix, using the principle of energy transfer from the sensitizer to the activator, color-tunable white light emission in a single host can be directly produced under the NUV excitation.⁸⁻¹⁰ More importantly, compared with the multiple emitting components of white-light LEDs system, the single-phased white-light-emitting phosphor for a NUV-pumped white-light LED would enable easy fabrication with perfect stability and color reproducibility.

As is well known, the emission and excitation spectra of Eu^{2+} ions usually consist of broad bands due to the transitions of $4f^7-4f^65d$,^{11,12} while the wide emission of

Mn²⁺ ions ranging from 500 to 700 nm depends on the crystal field of the host material. Because of the forbidden ⁴T₁₋₆A₁ transition, the emission efficiency of Mn²⁺ singly doped phosphor is low under UV excitation.^{13, 14} As a promising sensitizer for Mn²⁺ ions, Eu²⁺ ions have been applied in many Mn²⁺-doped hosts, such as Ca₁₂Al₁₄O₃₃Cl₂,⁸ Ca₉Y(PO₄)₇,¹⁵ and Ba₂Ca(B₃O₆)₂¹⁶ to improve the emission intensity of Mn²⁺. Moreover, white light can be realized by effective resonance-type energy transfer in this single-phased Eu²⁺/Mn²⁺ co-doping system, in which Mn²⁺ yields a red emission of d-d transition, while Eu²⁺ plays the role as both the activator to emit blue light and the sensitizer to Mn²⁺. Up till now, by adjusting the ratio of the sensitizer and the activator ions, white-light emission has been fabricated in multiple ions co-doped compounds of phosphates, silicates and aluminates.^{7, 17-20} However, the single-phased phosphor with highly effective luminescence, perfect stability, facility and low cost of synthesis is still to be explored.

Phosphates with the hexagonal apatite structure (space group *P6₃/m*, no. 176) are good host lattice for luminescence and laser materials. The characteristic tunnel in the structure allows for a variety of cationic and anionic substitutions, which leads to the modified apatite structures and variable composition of M₁₀(PO₄)₆X₂. M represents divalent cations (Ca²⁺, Sr²⁺, Ba²⁺) and X is monovalent anions (OH⁻, F⁻, Cl⁻). Rare earth (RE) or transition metal ions doped halophosphates are widely explored as red, green, and blue phosphors owing to advantages of relatively low sintering temperature, good chemical stability, and satisfactory absorption in the UV or NUV region.^{21, 22} The luminescent performance of these halophosphates phosphors is closely related to the halide anions and divalent cations in spite of the similar crystal structure.^{19, 23, 24} For instance, the energy-transfer efficiency from Eu²⁺ to Mn²⁺ in host lattice of Ca₉Lu(PO₄)₇,²⁵ (Sr₃, Ca, Ba)(PO₄)₃Cl²⁶ and Sr₅(PO₄)₃Cl²³ is different because the local surroundings of the sensitizers and the activators are influenced by the crystallinity, ions radii and anions electronegativity of the host materials.

In this paper, we synthesized a single-phased white-light-emitting phosphor Sr₅(PO₄)₃F co-doped with Eu²⁺, Mn²⁺. To further improve the luminescence efficiency of single-phased white-light-emitting phosphor, we also investigated the effect of

HBO₃, NaCl and KCl as flux in the synthesis on fluorescence performance. In our previous work, boric acid as flux has been found to greatly increase the blue-green fluorescence intensity of phosphors Ca_{12(0.97-x)}Al₁₄O₃₂F₂: 0.03Ce³⁺, xTb³⁺, ascribed to the improved crystallinity and partly substituting B³⁺ for Al³⁺ in the lattice.²⁷ We investigated the structure, luminescent properties and energy transfer mechanism of the single-phased white-light-emitting phosphor Sr₅(PO₄)₃F: Eu²⁺, Mn²⁺. With prominently increased photoluminescence efficiency, it may find promising application as a near ultraviolet-convertible direct white phosphor for white-light-emitting diodes.

2 Experimental

2.1 Sample Preparation. A series of Sr₅(PO₄)₃F: 0.02Eu²⁺, xMn²⁺ phosphors were synthesized by solid-state reaction. The raw material SrCO₃ (99.9%), NH₄F (99.9%), (NH₄)₂HPO₄ (99.9%), Eu₂O₃ (99.9%) and MnCO₃ (99.9%) were weighed according to the stoichiometric ratio. These powders were homogeneously mixed in an agate mortar for 30 min. The mixtures were transferred to a corundum crucible and then sintered in a tubular furnace at 1523K for 3 h under a reductive atmosphere (5% H₂+ 95% N₂ mixed flowing gas). When the temperature dropped to room temperature naturally, the polycrystalline products were obtained.

2.2 Measurements and Characterization. X-ray diffraction patterns (XRD) were collected on Bragg–Brentano diffractometer (Rigaku D/Max-2000, Rigaku Corporation, Tokyo, Japan) with monochromatic Cu K α radiation ($\lambda = 1.5418 \text{ \AA}$) of a graphite curve monochromator, and the data were collected from $2\theta = 10\text{-}80^\circ$ at a continuous scan rate of $4^\circ/\text{min}$ for phase identification, while structure refinement was carried out with $2\theta = 10\text{-}100^\circ$, step length of 0.02° and counting times of 5 s/step using the MAUD (Materials Analysis Using Diffraction) program.²⁸ The absorption spectra were measured on UV-vis-NIR spectrophotometer (Shimadzu UV-3600, Shimadzu Corporation, Kyoto, Japan) attached to an integral sphere using BaSO₄ as reference standard. The photoluminescence (PL) and photoluminescence excitation (PLE) spectra were measured by spectrofluorometer (Varian Cary-Eclipse 500, Varian Medical Systems Inc, Palo Alto, CA) with a 60 W xenon lamp as excitation source,

the excitation and emission slits were both set at 5.0 nm. All the measurements were carried out at room temperature under an identical condition.

2.3 Details of the Calculation. DFT calculations on the hexagonal $\text{Sr}_5(\text{PO}_4)_3\text{F}$ host and the Eu^{2+} , Mn^{2+} co-doped samples were carried out by using CASTEP code.²⁹ Geometry optimization and calculation of properties were performed to determine the crystal structure, electronic structure, and orbital population. The Vanderbilt ultrasoft pseudopotential with a cutoff energy of 340 eV was used, and k-points of $2 \times 2 \times 4$ was generated by using the Monkhorst–Pack scheme.³⁰ The exchange and correlation functions were treated by the local density approximation (GGA) in the formulation of PBE.^{31, 32} During the geometry optimization, lattice parameters and atomic positions were optimized simultaneously. For the self-consistent field iterations, the convergence tolerance for geometry optimization was selected with the differences in total energy, the maximal ionic Hellmann–Feynman force, the stress tensor, and the maximal displacement being within 1.0×10^{-5} eV/atom, 3.0×10^{-2} eV/Å, 5.0×10^{-2} GPa, and 1.0×10^{-3} Å, respectively.

3 Results and discussion

3.1 Phase identification and XRD refinement. A series of samples $\text{Sr}_5(\text{PO}_4)_3\text{F}:0.02\text{Eu}^{2+}, x\text{Mn}^{2+}$ with different content of Mn^{2+} ions ($x=0.02-0.06$) have been prepared in order to optimize the luminescent property. Powder XRD patterns in Figure 1 shows that all the as-prepared samples are identical and match well with the pure strontium fluorophosphate $\text{Sr}_5(\text{PO}_4)_3\text{F}$ (PDF# 50-1744), in hexagonal structure, $\text{P6}_3/\text{m}$ space group. When the molar ratio of Eu^{2+} ions fixed at 0.02, increasing Mn^{2+} ions up to $x=0.06$ does not cause significant change of structure. No diffraction peak of impurity is discerned, suggesting that the obtained samples are single phase. The Eu^{2+} and Mn^{2+} ions are incorporated into the lattice of $\text{Sr}_5(\text{PO}_4)_3\text{F}$.

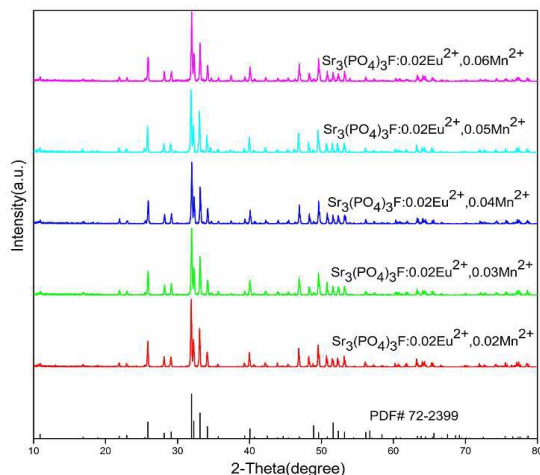


Figure 1 XRD patterns of $\text{Sr}_5(\text{PO}_4)_3\text{F}: 0.02\text{Eu}^{2+}$, $x\text{Mn}^{2+}$ ($x=0.02-0.06$) incorporated with different content of Mn^{2+} ions, respectively.

Based on XRD patterns, the lattice constants and atom positions of the samples $\text{Sr}_5(\text{PO}_4)_3\text{F}: 0.02\text{Eu}^{2+}$, $x\text{Mn}^{2+}$ ($x=0.02-0.06$) are refined by the MAUD suite program of Rietveld method using $\text{Sr}_5(\text{PO}_4)_3\text{F}$ as initial model (ICSD# 95737).³³ This series of materials crystallize in a hexagonal structure with P6_3 space group. As illustrated in Figure 2, Sr^{2+} ions reside in two Wyckoff sites. While 40% of Sr^{2+} ions (denoted as Sr1) dwell in Wyckoff 4f positions with C_3 point symmetry (Figure 2b), the other 60% (Sr2) populate in Wyckoff 6h positions with C_s point symmetry (Figure 2c). each Sr1 atom in the structure is surrounded by six O atoms forming a trigonal prism coordination. The $[\text{SrO}_6]$ trigonal prisms connect each other by sharing a plane of equilateral triangle on the trigonal prisms. Sr2 is coordinated by six O plus one F anion. $[\text{SrO}_6]$ trigonal prism, $[\text{SrO}_6\text{F}]$ polyhedron and $[\text{PO}_4]$ tetrahedron shares one corner with each other forming the framework of $\text{Sr}_5(\text{PO}_4)_3\text{F}$. When doped with Eu^{2+} and Mn^{2+} ions, they are supposed to substitute Sr^{2+} ions entering the 4f or 6h sites in $\text{Sr}_5(\text{PO}_4)_3\text{F}$ crystal structure due to the similar ionic radius and charge. In the refinement process, the dopants are assigned at the two Sr^{2+} sites, respectively. It is found that under the circumstances of both Mn^{2+} and Eu^{2+} at the Sr1 sites, the reliability parameters of refinement is optimum, which may suggest a preferring

occupation of Mn^{2+} and Eu^{2+} for the Sr1 sites. The corresponding refinement profiles of $\text{Sr}_5(\text{PO}_4)_3\text{F}$: 0.02Eu^{2+} , 0.05Mn^{2+} are presented in Figure 3. The reliability parameters of refinement on all the observed reflections as $R_p = 8.025\%$, $R_{wp} = 8.053\%$, $R_{exp} = 5.958\%$ and $\chi^2 = 1.12$ give a satisfied result, which also verifies the phase purity of the as-prepared sample $\text{Sr}_5(\text{PO}_4)_3\text{F}$: 0.02Eu^{2+} , 0.05Mn^{2+} .

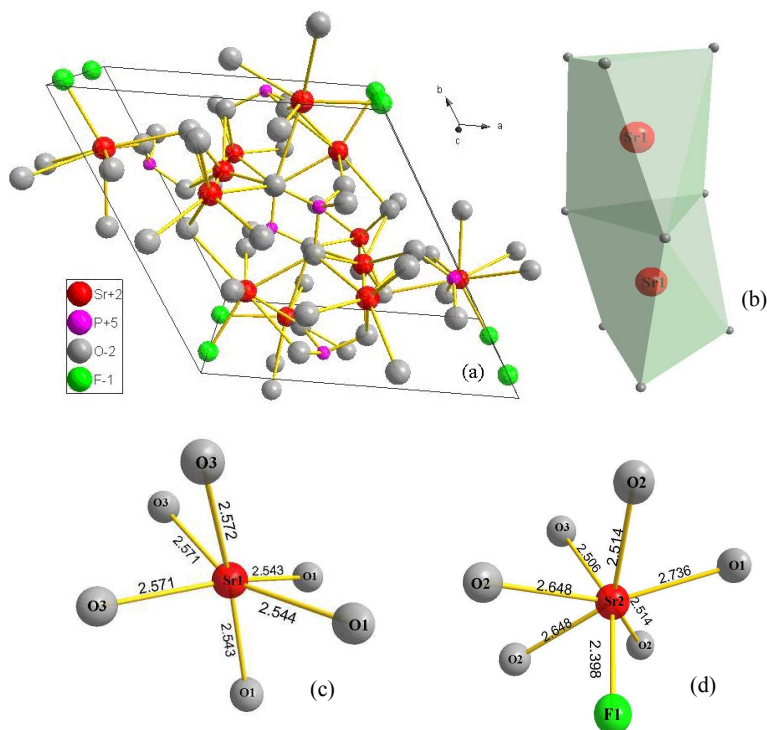


Figure 2 The crystal structure of $\text{Sr}_5(\text{PO}_4)_3\text{F}$ host (a), the connected trigonal prism coordination of Sr1 (b), and the coordination surroundings of Sr1 (c) and Sr2 (d) sites.

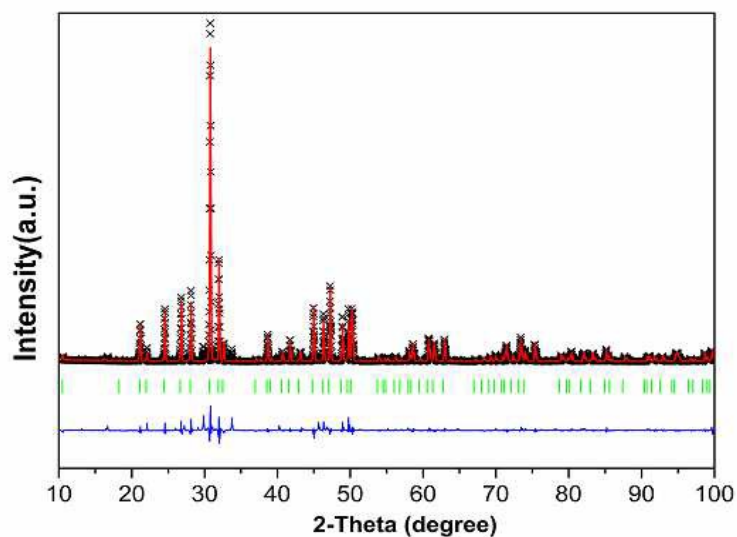


Figure 3 XRD refinement patterns of the samples $\text{Sr}_5(\text{PO}_4)_3\text{F}: 0.02\text{Eu}^{2+}, 0.05\text{Mn}^{2+}$, experimental (crosses), calculated (solid line), and difference (bottom).

The structural parameters and refinement factors of the host lattice and $\text{Sr}_5(\text{PO}_4)_3\text{F}: 0.02\text{Eu}^{2+}, 0.05\text{Mn}^{2+}$ are summarized in Table 1. From Table 1, it can be seen that with incorporation of Eu^{2+} and Mn^{2+} ions, the unit cell volume decreases, and with the Mn^{2+} content increasing to $x=0.06$, the cell volume drops to 591.10 \AA^3 (Figure 4). This phenomenon demonstrates the successful introduction of Eu^{2+} and Mn^{2+} into the structure of $\text{Sr}_5(\text{PO}_4)_3\text{F}$, which in turn leads to the shrinkage of unit cell volume, considering that both the ionic radii of Eu^{2+} and Mn^{2+} are smaller than that of Sr^{2+} under the given coordination number (Mn^{2+} 0.83, Eu^{2+} 1.17 while Sr^{2+} 1.18 \AA , for CN= 6, respectively).

Table 1 The structural parameters and refinement factors of the $\text{Sr}_5(\text{PO}_4)_3\text{F}$ -based samples

Formula	a/b (\AA)	c (\AA)	V(\AA^3)	R _{wp} (%)
$\text{Sr}_5(\text{PO}_4)_3\text{F}$	9.7327	7.2875	598.23	8.222
$\text{Sr}_5(\text{PO}_4)_3\text{F}: 0.02\text{Eu}^{2+}$	9.7289	7.2864	597.27	5.296
$\text{Sr}_5(\text{PO}_4)_3\text{F}: 0.02\text{Eu}^{2+}, 0.05\text{Mn}^{2+}$	9.6982	7.2569	591.10	8.053

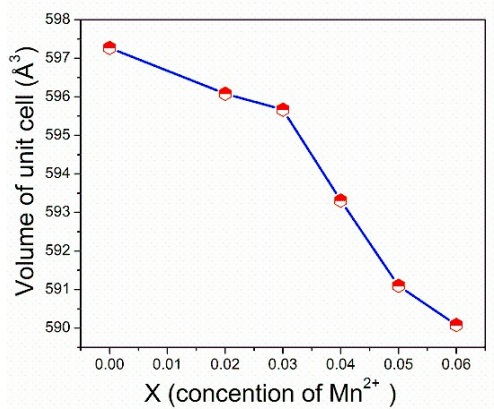


Figure 4 The dependence of lattice cell sizes on Mn^{2+} content for $\text{Sr}_5(\text{PO}_4)_3\text{F}: 0.02\text{Eu}^{2+}, x\text{Mn}^{2+}$ ($x = 0-0.06$).

3.2 Absorption spectra and Electronic Structure. The absorption spectra of $\text{Sr}_5(\text{PO}_4)_3\text{F}$ host and $\text{Sr}_5(\text{PO}_4)_3\text{F}: 0.02\text{Eu}^{2+}, x\text{Mn}^{2+}$ ($x=0-0.06$) phosphors are shown in Figure 5. The energy absorption of $\text{Sr}_5(\text{PO}_4)_3\text{F}$ host falls into the region less than 250 nm, indicating that there is no host absorption in NUV region. When Eu^{2+} ions are introduced into host, strong and broad absorption spectra from 250 to 430 nm in UV region appears, originating from $4f^7-4f^65d^1$ absorption of Eu^{2+} . For the Eu^{2+} and Mn^{2+} -codoped $\text{Sr}_5(\text{PO}_4)_3\text{F}: 0.02\text{Eu}^{2+}, x\text{Mn}^{2+}$ ($x=0-0.06$) samples, the absorption band is similar to that of Eu^{2+} singly doped sample except for the enhanced absorption intensity in the wavelength range of 230-430 nm by Mn^{2+} ions. The PLE spectra of $\text{Sr}_5(\text{PO}_4)_3\text{F}: 0.02\text{Eu}^{2+}, x\text{Mn}^{2+}$ in Figure 7 are in agreement with the absorption spectrum, indicating that the doubly doped phosphor may match well with NUV chips when used as WLEDs phosphor.

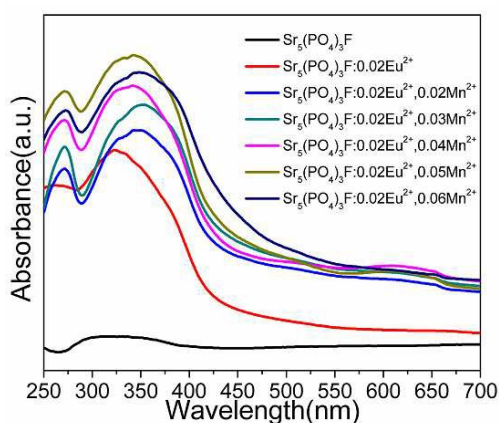


Figure 5 Absorption spectra of $\text{Sr}_5(\text{PO}_4)_3\text{F}: 0.02\text{Eu}^{2+}, x\text{Mn}^{2+}$ incorporated with different content of Mn^{2+} , respectively.

The absorption of the host lattices is related to the optical excitation of electrons from valence band (VBs) to the conduction band (CBs). Although an exact discussion of transitions from VBs to CBs requires calculation of the excited state electronic structure, the calculated static electronic band, as an approximation, may still provide important information. The calculated band structure in Figure 6a revealed that hexagonal $\text{Sr}_5(\text{PO}_4)_3\text{F}$ host is broad band gap materials with direct band gap energy 5.099 eV. From Figure 6b, it can be seen that with $\text{Eu}^{2+}/\text{Mn}^{2+}$ co-doped, some

interband forms at the top of VB, and the band gap energy decreased to 3.035 eV. The interband transition could be ascribed to the charge transfer from O-2p to Eu-4f5d and Mn 3d orbitals,³⁴ basically corresponding to the excitation energy of Mn²⁺ in Figure 7a. According to the orbital population analysis, the VBs of the host lattice are dominated by the 2p orbitals of O atoms, and the CBs consist of O2p plus O3d orbitals. For Eu²⁺/Mn²⁺ co-doped Sr₅(PO₄)₃F, Mn3d and Eu 5d orbitals blend into the upper energy parts of VBs and the bottom of CBs (Figure 6b). In addition, with the formation of the interbands, the number of the upper CBs bands decreases because the orbitals of Mn3d and Eu5d with O2p is mixed and homogenized.

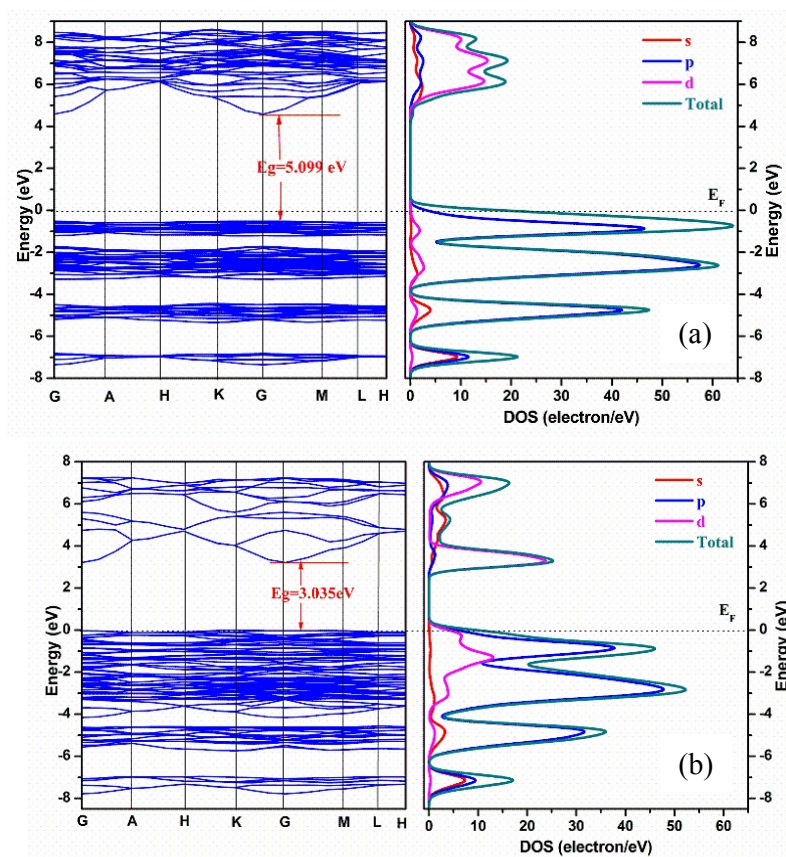


Figure 6 Calculated band structures (left) and orbital populations (right) of Sr₅(PO₄)₃F (a) and Sr₅(PO₄)₃F: 0.02Eu²⁺, 0.05Mn²⁺ (b) near the Fermi energy (E_F) level. The Fermi energy is the zero of the energy.

3.3 Photoluminescence Properties. Figure 7 shows the excitation and emission spectra of Eu^{2+} , Mn^{2+} singly and co-activated $\text{Sr}_5(\text{PO}_4)_3\text{F}$ phosphor. Upon excitation of 405 nm, the Mn^{2+} ions singly doped sample of $\text{Sr}_5(\text{PO}_4)_3\text{F}: 0.05\text{Mn}^{2+}$ shows a weak yellow emission peak at 556 nm assigned to the ${}^4\text{T}_{1g}(\text{G})\text{--}{}^6\text{A}_{1g}(\text{S})$ spin-forbidden transition of Mn^{2+} ions (Figure 7a). For Eu^{2+} activated $\text{Sr}_5(\text{PO}_4)_3\text{F}: 0.02\text{Eu}^{2+}$, the emission band centered at 440 nm is ascribed to the $4f^7\text{--}4f^65d^1$ electronic transition of Eu^{2+} ions. Monitored by the emission at 440 nm, the PLE spectrum of $\text{Sr}_5(\text{PO}_4)_3\text{F}: 0.02\text{Eu}^{2+}$ exhibits a broad excitation band from 250 to 430 nm summit at 294 nm (Figure 7b). Compared Figure 7a and 7b, the overlap of excitation spectra is readily observed between $\text{Sr}_5(\text{PO}_4)_3\text{F}: 0.02\text{Eu}^{2+}$ and $\text{Sr}_5(\text{PO}_4)_3\text{F}: 0.05\text{Mn}^{2+}$, which indicates the possibility of an effective resonance-type energy transfer (ET) from Eu^{2+} to Mn^{2+} ions.²² Therefore, a highly efficient luminescence of Eu^{2+} , Mn^{2+} co-activated $\text{Sr}_5(\text{PO}_4)_3\text{F}: 0.02\text{Eu}^{2+}$, 0.05Mn^{2+} phosphor (in Figure 7c) can be fabricated under the broad excitation in the range of 250 to 430 nm. The emission color can be trimmed by adjusting the ratio between Mn^{2+} and Eu^{2+} ions in the host lattice.

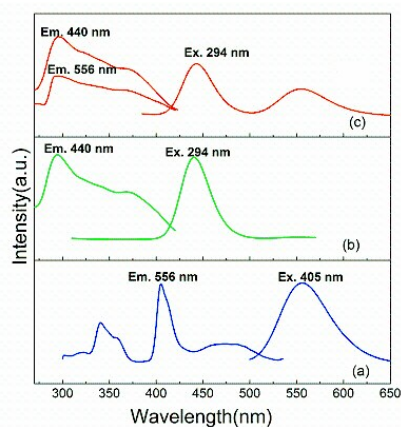


Figure 7 PLE and PL spectra of $\text{Sr}_5(\text{PO}_4)_3\text{F}: 0.005\text{Mn}^{2+}$ (a), $\text{Sr}_5(\text{PO}_4)_3\text{F}: 0.02\text{Eu}^{2+}$ (b), and $\text{Sr}_5(\text{PO}_4)_3\text{F}: 0.02\text{Eu}^{2+}$, 0.05Mn^{2+} (c).

Figure 8a displays the dependence of emission intensity of $\text{Sr}_5(\text{PO}_4)_3\text{F}: 0.02\text{Eu}^{2+}$, $x\text{Mn}^{2+}$ on different Mn^{2+} doped concentration ($x=0.02\text{--}0.06$) under 365 nm excitation. It can be found that with increasing Mn^{2+} doped concentration, the emission intensity of Mn^{2+} at 556 nm enhances, whereas that of Eu^{2+} at 440 nm decreases remarkably,

attributed to the enhancing energy transfer from Eu^{2+} to Mn^{2+} . The emission intensity at 556 nm increases until the doped concentration of Mn^{2+} ions reaches 0.05. Above this Mn^{2+} concentration, the emission intensity decreases due to the concentration quenching effect resulting from the interaction between the Mn^{2+} ions.^{35,36} The CIE chromaticity coordinates of the series of $\text{Sr}_5(\text{PO}_4)_3\text{F}: 0.02\text{Eu}^{2+}, x\text{Mn}^{2+}$ ($x=0.02-0.06$) under excitation of 365 nm are shown in Figure 8b.

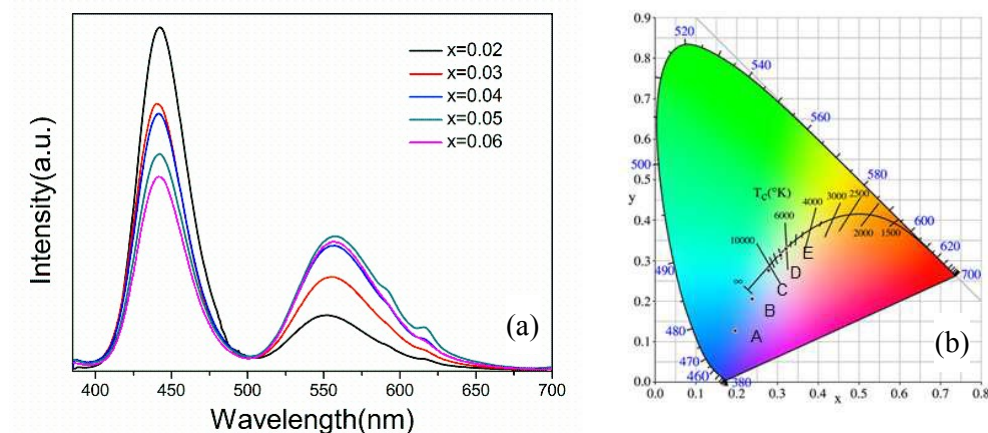


Figure 8 PL (a) and CIE chromaticity coordinates (b) of $\text{Sr}_5(\text{PO}_4)_3\text{F}: 0.02\text{Eu}^{2+}, x\text{Mn}^{2+}$ phosphors excited at 365 nm with different Mn^{2+} contents ($y= 0.02, 0.03, 0.04, 0.05,$ and 0.06).

It is generally accepted that the energy transfer from the sensitizer Eu^{2+} to activator Mn^{2+} in the host is realized via a resonance-type energy transfer mechanism derived from electric multipolar interaction.^{37, 38} According to Dexter's energy transfer expressions of multi-polar interaction and Reisfeld's approximation,³⁹⁻⁴¹ the following relation can be given as follows:

$$\frac{\eta_0}{\eta_s} \propto C_{\text{Mn}^{2+}}^{n/3} \quad (1)$$

In the formula, η_0 and η_s are the luminescence quantum efficiency of Eu^{2+} in the absence and presence of Mn^{2+} , respectively. The value of the η_0/η_s can be estimated approximately by the ratio of the relative luminescence intensity I_{s0}/I_s of Eu^{2+} , which is proportional to the total concentration of Mn^{2+} , and $n=6, 8,$ and 10 correspond to electric multipolar interaction of electric dipole-dipole, dipole-quadrupole and

quadrupole–quadrupole interactions, respectively. The relationships between I_{s0} / I_s and $C_{Mn^{2+}}^{n/3}$ are illustrated in Figure 9. By comparing the R values of fitting factors, the optimal linear relationship is obtained from $I_{s0} / I_s \propto C_{Mn^{2+}}^{6/3}$ in Figure 9a ($R = 0.9885$), which implies that the energy transfer from Eu^{2+} to Mn^{2+} occurs following a dipole-dipole interaction.

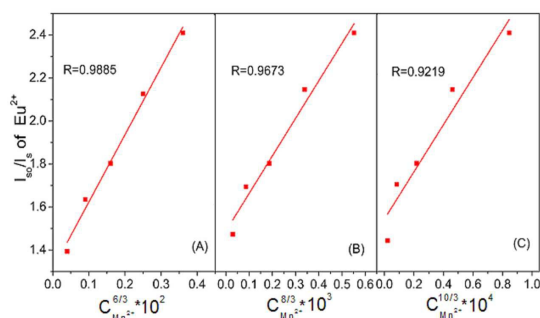


Figure 9 The relationships between I_{s0} / I_s and $C_{Mn^{2+}}^{n/3}$.

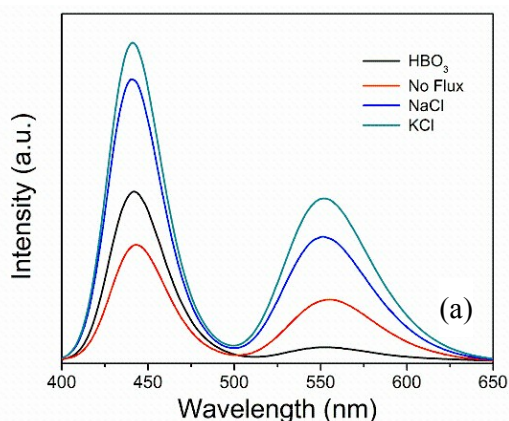
The critical distance of energy transfer from Eu^{2+} to Mn^{2+} is calculated by the concentration quenching method, in which the critical distance $R_{(Eu-Mn)}$ between Eu^{2+} and Mn^{2+} is determined based on geometrical consideration by the formula proposed by Blasse.⁴⁰

$$R_{Eu-Mn} = 2 \left[\frac{3V}{4\pi x_c N} \right]^{1/3} \quad (2)$$

In the formula, V is the volume of the unit cell, and N is the number cations in the unit cell of host, and x_c is the critical concentration, the total concentration of sensitizer ions Eu^{2+} and activator ions Mn^{2+} . According to the crystal structure analysis of $Sr_5(PO_4)_3F: 0.02Eu^{2+}, 0.05Mn^{2+}$, the values of V and N are 591.1 \AA^3 and 10, respectively. The critical concentration $x_{c(Eu^{2+}+Mn^{2+})}$ is 0.07, and thus the critical distance R_c is calculated to be 11.72 \AA .

3.4 The influence of fluxes on fluorescence. The effect of various fluxes in synthesis on the luminescent performance of phosphor has been reported in many references.^{42, 43} In order to improve the emission intensity of $Sr_5(PO_4)_3F: 0.02Eu^{2+}$,

$x\text{Mn}^{2+}$, different fluxes with double molar amount of the final fluorophosphate compound were added in synthesis of phosphors. From Figure 10a, it can be found that the photoluminescence intensity of phosphor $\text{Sr}_5(\text{PO}_4)_3\text{F}: 0.02\text{Eu}^{2+}, 0.05\text{Mn}^{2+}$ are prominently enhanced by KCl, NaCl, and H_3BO_3 , among which KCl presents the optimum promotion effect. Figure 10b shows that the PL intensity of $\text{Sr}_5(\text{PO}_4)_3\text{F}: 0.02\text{Eu}^{2+}, 0.05\text{Mn}^{2+}$ is drastically enhanced when the phosphor is prepared with twice molar KCl as flux. The PL intensity increases by 85% compared with the sample synthesized without flux added. The influence of fluxes on the photoluminescence property has been ascribed to three aspect: (1) the flux of low melting point facilitate activator ions enter to the host lattice; (2) the improved crystallinity of the host material reduces the nonradiative loss in the energy transfer process; (3) partial cations or anions in the flux replace the host ions and disturb surrounding of the activators. It was reported that when H_3BO_3 was used as flux for synthesis of phosphor, parts of B^{3+} replaced Al^{3+} in the lattice due to the similar radius, which result in the increasing of photoluminescence intensity for aluminates and fluoroaluminates phosphors. Herein, the effect of KCl on fluorescence performance may be ascribed to both the improvement of the crystallinity of the host and K^+ entering the crystallographic sites of Sr^{2+} , because EDS analysis demonstrates the existence of a slightly small amount of K^+ in $\text{Sr}_5(\text{PO}_4)_3\text{F}: 0.02\text{Eu}^{2+}, 0.05\text{Mn}^{2+}$ phosphor. We have inspected the change of lattice cell after K^+ entering the $\text{Sr}_5(\text{PO}_4)_3\text{F}$ structure by Rietveld refinement. However, the change is extremely slight, due to the similar radii of K^+ and Sr^{2+} and the small amount of K^+ ions.



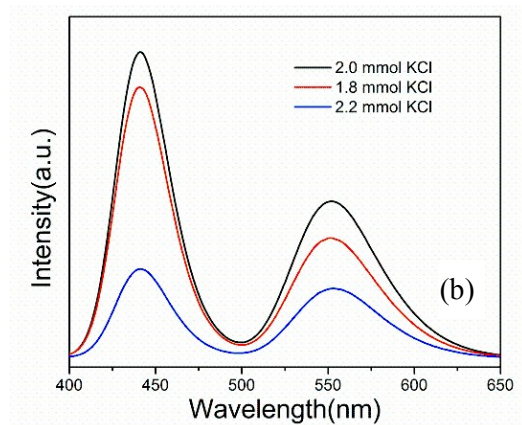


Figure 10 Under 365 nm excitation, PL emission spectra of $\text{Sr}_5(\text{PO}_4)_3\text{F}:0.02 \text{Eu}^{2+}$, 0.05Mn^{2+} synthesized (a) in the presence of different fluxes (NaCl , KCl and HBO_3); (b) Under the different adding amount of KCl at 1523K.

4 Conclusion

A series of single-phased phosphors $\text{Sr}_5(\text{PO}_4)_3\text{F}: 0.02\text{Eu}^{2+}$, $x\text{Mn}^{2+}$ ($x=0.02-0.06$) with hexagonal structure, $\text{P6}_3/\text{m}$ space group have been synthesized by high-temperature solid state reaction. The crystal structure is analyzed by X-ray diffraction. The energy band structure of $\text{Sr}_5(\text{PO}_4)_3\text{F}$ and the $\text{Eu}^{2+}/\text{Mn}^{2+}$ co-doped sample were analyzed by density functional theory calculation (DFT). The energy transfer process from Eu^{2+} to Mn^{2+} ions and the possible energy transfer mechanism were investigated by absorption spectra, photoluminescence and photoluminescence excitation spectra. The excitation spectrum of the obtained phosphors exhibits a broad excitation band in the wavelength range of 250 - 430 nm, which is matchable with NUV LED chips. The efficient photoluminescence of phosphors $\text{Sr}_5(\text{PO}_4)_3\text{F}: 0.02\text{Eu}^{2+}$, $x\text{Mn}^{2+}$ ($x=0.02-0.06$) is ascribed to the effective energy transfer from the Eu^{2+} to Mn^{2+} ions by co-doping Eu^{2+} and Mn^{2+} ions in the host lattice. Moreover, the PL intensity of $\text{Sr}_5(\text{PO}_4)_3\text{F}: 0.02\text{Eu}^{2+}$, 0.05Mn^{2+} is drastically enhanced by 85% when the phosphor

is prepared with twice molar KCl as flux. The CIE chromate shows the emissive colors can be adjusted from blue to white by altering the ratio of Eu^{2+} and Mn^{2+} doped in the host. The energy transfer mechanism from the Eu^{2+} to Mn^{2+} ions is a resonant type via a nonradiative dipole–dipole interaction. The critical distance has been calculated to be about 11.72 Å. The above observations hint a promising application of $\text{Sr}_5(\text{PO}_4)_3\text{F}: 0.02\text{Eu}^{2+}, 0.05\text{Mn}^{2+}$ as a single-phased white-light-emitting phosphor under NUV irradiation.

Acknowledgments

This work is supported by the Program of Shanghai Normal University (DZL124).

References

1. S. Pimputkar, J. S. Speck, S. P. DenBaars and S. Nakamura, *Nat Photon*, 2009, 3, 180-182.
2. S. Tonzani, *Nature*, 2009, 459, 312-314.
3. S. Nakamura, *III-Vs Review*, 1998, 11, 28-32.
4. H. Liang, Q. Zeng, Z. Tian, H. Lin, Q. Su, G. Zhang and Y. Fu, *J. Electrochem. Soc.*, 2007, 154, J177-J180.
5. Y. Liu, W. Zhuang, Y. Hu and W. Gao, *J. Rare Earths.*, 2010, 28, 181-184.
6. V. Bachmann, C. Ronda and A. Meijerink, *Chem. Mater.*, 2009, 21, 2077-2084.
7. N. Guo, Y. Zheng, Y. Jia, H. Qiao and H. You, *J. Phys. Chem. C*, 2012, 116, 1329-1334.
8. W. Lv, W. Lü, N. Guo, Y. Jia, Q. Zhao, M. Jiao, B. Shao and H. You, *RSC Adv.*, 2013, 3, 16034.
9. G. Zhu, S. Xin, Y. Wen, Q. Wang, M. Que and Y. Wang, *RSC Adv.*, 2013, 3, 9311.
10. H. Liu, Y. Luo, Z. Mao, L. Liao and Z. Xia, *J. Mater. Chem. C*, 2014, 2, 1619.
11. Y. C. Chiu, W. R. Liu, C. K. Chang, C. C. Liao, Y. T. Yeh, S. M. Jang and T. M. Chen, *J. Mater. Chem.*, 2010, 20, 1755.
12. M. P. Saradhi and U. V. Varadaraju, *Chem. Mater.*, 2006, 18, 5267-5272.
13. D. Zhang, C. Wang, Y. Liu, Q. Shi, W. Wang and Y. Zhai, *J. Lumin.*, 2012, 132, 1529-1531.
14. M. Peng, X. Yin, P. A. Tanner, C. Liang, P. Li, Q. Zhang, J. Qiu and A. Srivastava, *J. Am.*

- Ceram. Soc.*, 2013, 96, 2870-2876.
15. C. H. Huang, P. J. Wu, J. F. Lee and T.-M. Chen, *J. Mater. Chem.*, 2011, 21, 10489.
 16. F. Xiao, Y. N. Xue, Y. Y. Ma and Q. Y. Zhang, *Phys. B: Condens. Matter.*, 2010, 405, 891-895.
 17. W. Wu and Z. Xia, *RSC Adv.*, 2013, 3, 6051-6057.
 18. X. Zheng, Q. Fei, Z. Mao, Y. Liu, Y. Cai, Q. Lu, H. Tian and D. Wang, *J. Rare Earths*, 2011, 29, 522-526.
 19. N. Guo, Y. Jia, W. Lu, W. Lv, Q. Zhao, M. Jiao, B. Shao and H. You, *Dalton Trans.*, 2013, 42, 5649-5654.
 20. Z. Lin, X. Liang, Y. Ou, C. Fan, S. Yuan, H. Zeng and G. Chen, *J. Alloys Compd.*, 2010, 496, L33-L37.
 21. Q. Zeng, H. Liang, G. Zhang, M. D. Birowosuto, Z. Tian, H. Lin, Y. Fu, P. Dorenbos and Q. Su, *J. Phys.: Condens. Matter*, 2006, 18, 9549-9560.
 22. K. Li, D. Geng, M. Shang, Y. Zhang, H. Lian and J. Lin, *J. Phys. Chem. C.*, 2014, 118, 11026-11034.
 23. C. Guo, L. Luan, X. Ding, F. Zhang, F. G. Shi, F. Gao and L. Liang, *Appl. Phys. B*, 2009, 95, 779-785.
 24. Z. Fu, X. Wang, Y. Yang, Z. Wu, D. Duan and X. Fu, *Dalton Trans.*, 2014, 43, 2819-2827.
 25. N. Guo, Y. Huang, H. You, M. Yang, Y. Song, K. Liu and Y. Zheng, *Inorg. Chem.* 2010, 49, 10907-10913.
 26. X. Chen, P. Dai, X. Zhang, C. Li, S. Lu, X. Wang, Y. Jia and Y. Liu, *Inorg. Chem.*, 2014, 53, 3441-3448.
 27. H. Ling, J. Huang, B. Hou, J. Liu, X. Yu and J. Ballato, *J. Am. Ceram. Soc.*, 2014, 97, 2116-2123.
 28. L. Lutterotti, S. Matthies and H.-R. Wenk, presented in part at the Proceeding of the Twelfth International Conference on Textures of Materials (ICOTOM-12), Ottawa, Canada, 1999.
 29. M. D. Segall, J. D. L. Philip, M. J. Probert, C. J. Pickard, P. J. Hasnip, S. J. Clark and M. C. Payne, *J. Phys.: Condens. Matter.*, 2002, 14, 2717-2722.
 30. H. J. Monkhorst and J. D. B. Pack, *Phys. Rev.*, 1976, 13, 5188-5192.
 31. D. M. Ceperley and B. Alder, *J. Phys. Rev. Lett.*, 1980, 45, 566-569.
 32. J. P. Perdew and A. Zunger, *Phys. Rev. B.*, 1981, 23, 5048-5079.

33. S. H. Swafford and E. M. Holt, *Solid State Sci.*, 2002, 4, 807-812.
34. G. Blasse and A. Bril, *J. Chem. Phys.*, 1966, 45, 2350-2355.
35. D. R. Tallant, M. P. M. and J. C. Wright, *J. Chem. Phys.*, 1976, 65, 510-521.
36. G. Blasse and B. C. Grabmaier, *Energy Transfer in Luminescent Materials*, Springer Press, Berlin, 1994.
37. M. P. Miller and J. C. Wright, *J. Chem. Phys.*, 1979, 71, 324-338.
38. H. P. You, J. L. Zhang and H. J. Zhang, *J. Phys. Chem. C*, 2007, 111, 10657-10661.
39. R. Reisfeld and N. L. Soffer, *J. Solid State Chem.*, 1979, 28, 391-395.
40. G. Blasse, *Phys. Lett.*, 1968, 28, 444-445.
41. C. H. Huang and T. M. Chen, *J. Phys. Chem. C*, 2011, 115, 2349-2355.
42. X. Teng, W. Zhuang, Y. Hu, C. Zhao, H. He and X. Huang, *J. Alloys Compd.*, 2008, 458, 446-449.
43. S. Shi, J. Gao and J. Zhou, *Opt. Mater.*, 2008, 30, 1616-1620.